An Experimental Study on the Control of Slotless Self-Bearing Motor Using Nonlinear Control

Vo Duc Nhan
Institute for Control Engineering and Automation
Hanoi University of Science and Technology
Hanoi, Vietnam
voducnhanqn@gmail.com

Nguyen Xuan Bien
Faculty of Mechanical Engineering
Thuy Loi University
Hanoi, Vietnam
xuanbien96@gmail.com

Nguyen Quang Dich
Institute for Control Engineering and Automation
Hanoi University of Science and Technology
Hanoi, Vietnam
dichnq@gmail.com

Vo Thanh Ha
Faculty of Electrical and Electrical Engineering
University of Transport and Communications
Hanoi, Vietnam
vothanhha.ktd@utc.edu.vn

Abstract-This article presents a Slotless Self-Bearing Motor (SSBM) with a six-phase coil stator instead of an iron core. The rotor consists of a permanent magnet and an encased iron yoke. The magnetic forces caused by the interplay between the stator currents and the magnetic field govern the rotational speed and radial position of the rotor. An SSBM mathematical model and its control method are also included in this study. This motor is controlled by field-oriented control. Theoretical analysis of magnetic force and moment characteristics is performed, and a control approach is provided. Sliding-mode control is a control technique that is simple, and effective and is used to assist the control system in approaching the reference value. It is also widely utilized to control the position and speed of the motor. The findings were constructed and validated using experiment-confirmed analytical data to prove the proposed control strategy.

Keywords-FOC; Slotless Self-Bearing Motor; sliding mode control; PI; PID

I. INTRODUCTION

The quality of a powertrain depends on the engine. Creating a transmission system capable of smooth speed change with a wide adjustment range and high accuracy of the adjustment quantity in static mode is necessary to create a working area with negligible error. Working with any transition process must achieve increased stability, and the system must be able to respond quickly to adjustment requirements [1-3]. All these make more stringent the requirements on powertrains. Also, special needs for intelligent and fast control in synchronous motors will be significantly enhanced. Conventional motor structures have been greatly improved. However, there are still disadvantages of an engine with a steel core, such as the existence of pulsating torque and low operating frequency [3-5]. So, the steel coreless self-lifting motor is a significant invention that minimizes the frictional force between the rotating shaft in the machine part, helping the effortless movement for better performance in motion applications of engineering disciplines [6-8]. Brushless motors have many advantages such as high speed, fast acceleration, and constant torque (Figure 1) and higher continuity, low noise, and less electromagnetic interference (Figure 2) [9-11].
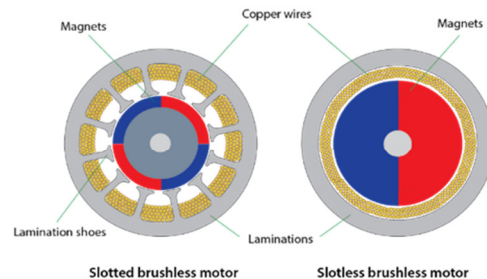
Fig. 1.   Comparison of the engine structure with and without steel core.

The cogging torque can be reduced by improving the stator grooves and the magnet pole exerts. A 6-phase coreless steel lifter motor comprises of a cylindrical two-pole magnet, a surrounding iron shell, a rotating shaft, and an aluminum base that connects the engine's components. The distance of the air gap between the magnet and the iron case remains constant to ensure a stable magnetic field of the magnet pole. As a result, the magnetic lines of force leaving the surface of interest tend to rotate towards the south pole. In other words, the magnetic lines of the staff will come out perpendicular to the tangent at that point, creating an even distribution of the magnetic field between the rotor and the stator. In addition, in this motor, the increase in the number of teeth on the stator makes for more interaction, and they create pairs of forces that cancel each other, thereby also reducing the cogging torque [11-13]. The SSBM in the experimental set motors is shown in Figure 3.

Corresponding author: Vo Thanh Ha
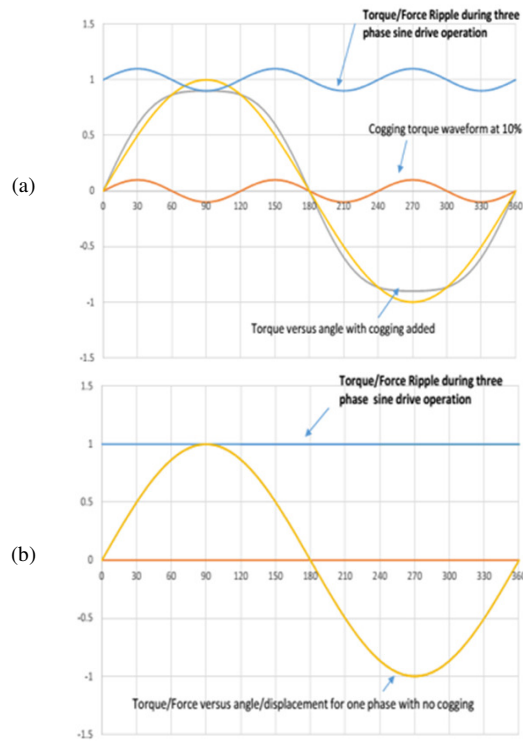
Fig. 2.   Torque comparison of two types of motors: (a) Motor with steel core, (b) motor without steel core.
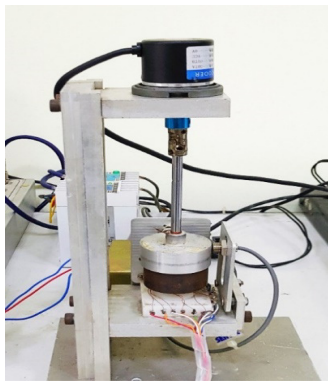
Fig. 3.   The SSBM in the experimental set motors.

This motor creates torque [14-16] and lift will be done by giving the supplied current. Thus, Lorentz force is generated. According to Newton's theorem, since the coil is at rest, the reaction forces acting on the motor rotor have opposite directions. This force consists of two components, one that generates lift and the other that creates rotor torque. When any current (positive or negative) is applied to a phase, a pair of forces is generated whose direction depends on its position relatively to the rotor. Thus, the torque and lift can be controlled by varying the amplitude and phase of the current in the stator. Consequently, the construction of the controller is required to improve system quality. A PI controller handles speed control, whereas a PID handles displacement position control [17-23]. The actual speed is close to the reference value and reacts effectively. When there is a load torque, the controller boosts or cuts the current to help minimize the divergence. The phase stator currents take on a sinusoidal

shape following the speed change. In addition, the actual speed is responsive and close to the reference value. The controller boosts or reduces the current to minimize divergence when a load torque is present. As a result, the phase stator currents take on a sinusoidal shape when the speed changes. On the other hand, the total rotor displacements jump from 0s to 0.1s. This signifies that the rotor is still centered in the stator. As a result, the controller promptly corrects the align deviation when applying external pressures. However, the rotor's speed and displacement overshoot during the transition point. Consequently, it has been reported that a Sliding Mode Control (SMC) system could be used to improve control quality. SMC is a control method that forces the system's trajectory onto the sliding surface using a high-speed switching control rule. Sliding-mode control is widely used in practical applications [24-27], because of its benefits, such as ease of implementation, finite-time convergence, excellent dynamic responsiveness, and robustness against parameter variations and disturbances. Furthermore, the stability of sliding-mode control may offer flawless tracking even when parameters or model errors are present, based on the design of a bearingless motor's SMC and *dq* axis current regulation [28-34]. Consequently, this SSBM outperforms the PID controller in position and speed control. Thus, the sliding-mode control will be chosen to design this motor's speed and position controller.

II.   MATHEMATICAL MODEL

The stator currents are supplied as [17]:

$$\begin{cases} i_{a,d} = i_d \cos(\psi) + i_q \sin(\psi) \pm A_m \cos(\phi_m) \\ i_{b,e} = i_d \cos(\psi - 2\pi/3) + i_q \sin(\psi - 2\pi/3) \pm A_m \cos(\phi_m + \pi/3) \\ i_{c,f} = i_d \cos(\psi - 4\pi/3) + i_q \sin(\psi - 4\pi/3) \pm A_m \cos(\phi_m + 2\pi/3) \end{cases} \quad (1)$$

where i_d is the direct axis current, i_q is the quadrate axis current, ψ is the angular position of the rotor, A_m is the amplitude of the motor current, and ϕ_m is its phase.

We combine (1) with the stator winding properties to calculate the total force acting on the rotor and the generated torque. The rotating torque and bearing forces in case of turns are:

$$\begin{cases} \tau = k_{nm} k_m A_m \sin(\phi_m - \psi + \theta_0 + \pi/4) \\ f_x = -k_{nb} k_b \left\{ i_d \sin(2\theta_0) - i_q \cos(2\theta_0) \right\} \\ f_y = k_{nb} k_b \left\{ i_d \cos(2\theta_0) + i_q \sin(2\theta_0) \right\} \end{cases} \quad (2)$$

where τ is the rotating torque, f_x and f_y are bearing forces, B is the amplitude of the magnetic flux density, l_p is the length of the parallel part of the winding, l_t is the length of the serial part of the winding, n is the total number of turns, and θ_0 is the angular position of the +a-phase winding. It must be an odd number so that the wires do not overlap.

From (2), the mathematical model of the SSBM is completely constructed with force and torque equations. Next, the control system for the SSBM will be designed.

$$\begin{cases} k_m = -\left(3\sqrt{2}l_p + \dfrac{8(6-3\sqrt{2})}{\pi}l_t\right)rB \\[2mm] k_b = -\left(3l_p + \dfrac{12}{\pi}l_t\right)B \\[2mm] k_{nm} = 1 + 2\cos\left(\dfrac{\pi}{3n}\right) + 2\cos\left(2\dfrac{\pi}{3n}\right) + \cdots + 2\cos\left(\dfrac{(n-1)}{2}\dfrac{\pi}{3n}\right) \\[2mm] k_{nb} = 1 + 2\cos\left(2\dfrac{\pi}{3n}\right) + 2\cos\left(4\dfrac{\pi}{3n}\right) + \cdots + 2\cos\left((n-1)\dfrac{\pi}{3n}\right) \end{cases} \quad (3)$$

III. DESIGNING THE CONTROL SYSTEM

A. Control Structure

When the angular position of the rotor can be obtained, the stator current can be calculated by (1) and the force and torque by (2). The θ_0 is the angular position of the +a-phase winding so if the +a-phase coincides with the x-axis then $\theta_0=0$. φ_m is the phase of the torque current and depends on control strategy. To conduct the clear control algorithm, we can assume that $\theta_0 = 0$ and $\phi_m = \psi + \dfrac{\pi}{4}$ or $\phi_m - \psi + \theta_0 + \dfrac{\pi}{4} = \dfrac{\pi}{2}$. Then, (2) becomes:

$$\begin{cases} \tau = k_{nm}k_m A_m \\ F_x = k_{nb}k_b i_q \\ F_y = k_{nb}k_b i_d \end{cases} \quad (4)$$

It is easy to see that the rotating torque is produced by A_m and the bearing force is produced by i_d and i_q. Therefore, the rotating torque can be controlled by A_m and the bearing force by i_d and i_q. On the other hand, the two components, force and torque, are mathematically independent from each other, thus, the control structure is introduced as shown in Figure 3. The SMC is used for both the speed control and the displacement position control. SMC is a well-known powerful control scheme which has been successfully and widely applied for both linear and nonlinear systems. In this study, the linear sliding mode which uses the linear sliding surface has been used to design the speed and position controller.

Settings: $K_T = k_{nm}k_m$ and $K_{fx} = K_{fy} = k_{nb}k_b$, and (4) becomes:

$$\begin{cases} \tau = K_T A_m \\ F_x = K_{fx} i_q \\ F_y = K_{fy} i_d \end{cases} \quad (5)$$

The dynamic equation of the rotor is:

$$\tau - T_l = J\frac{d\omega}{dt} \quad (6)$$

$$F - F_l = Ma \quad (7)$$

where M is the weight of the rotor, a is the acceleration of the rotor, T_l is the load torque and F_l is the load force.

B. Designing the Position Controller

Assuming the effect of load torque and load force are the same as external disturbances, the mathematical model of the motor can be expressed as [17]:

$$\begin{cases} \ddot{x} = \dfrac{K_{fx}}{m}i_q \\[2mm] \ddot{y} = \dfrac{K_{fy}}{m}i_d \\[2mm] \dot{\omega} = \dfrac{K_T}{J}A_m \end{cases} \quad (8)$$

The parameters of the two equations that generate the bearing force are the same. Thus, a sliding controller for both positions along the x and y axes is designed. The settings in the model in (8) are:

$$K_f = \frac{K_{fx}}{m} = \frac{K_{fy}}{m}, u_d = K_f i_d, u_q = K_f i_q \quad (9)$$

We suppose that the controlled object is only a double integral $1/s^2$, the SMC is used for calculating parameters u_d and u_q and then we return to calculate the current parameters i_d and i_q. The controlled object $1/s^2$ is expressed as follows:

$$\frac{dx}{dt} = \begin{pmatrix} x_2 \\ u \end{pmatrix} \text{ and } y = x_1 \quad (10)$$

where $\underline{x} = \begin{pmatrix} x_1 \\ x_2 \end{pmatrix}$ is the state vector, $\underline{y}$ is the output signal and $u = u_d = u_q$ is the control input. The most commonly used sliding surface is the linear sliding surface which is:

$$s_1(e) = a_0 e_1 + e_2 \text{ and } \frac{de_1}{dt} = e_2 \quad (11)$$

where e_1 is the position error and a_0 is a positive design parameter chosen such that the polynomial $P(s) = a_0 + s$ is a Hurwitz polynomial which has real parts of the roots smaller than zero.

To guarantee the stability of the system, the Lyapunov stability theory is used. The Lyapunov function has the form of:

$$V(s_1) = \frac{1}{2}s_1^2 \quad (12)$$

Then, the control design task becomes to make $\dot{V}(s_1) < 0$ in the neighborhood of the equilibrium. Thus, we have:

$$\frac{dV(s_1)}{dt} < 0 \Leftrightarrow s_1 \frac{ds_1}{dt} < 0 \Leftrightarrow \frac{ds_1}{dt}\text{sgn}(s_1(e)) < 0 \quad (13)$$

On the other hand:

$$\frac{ds_1}{dt} = a_0 \frac{de_1}{dt} + \frac{de_2}{dt} = a_0 \frac{de_1}{dt} - u \quad (14)$$

Thus, (13) becomes:

$$(a_0 \frac{de_1}{dt} - u)\text{sgn}(s_1(e)) < 0 \quad (15)$$

$$\Leftrightarrow a_0 \frac{de_1}{dt} - u = \begin{cases} < 0 & if \quad s_1(e) > 0 \\ > 0 & if \quad s_1(e) < 0 \end{cases} \quad (16)$$

$$\Leftrightarrow u = \begin{cases} > a_0 \frac{de_1}{dt} & if \quad s_1(e) > 0 \\ < a_0 \frac{de_1}{dt} & if \quad s_1(e) < 0 \end{cases} \quad (17)$$

Choosing the control input u:

$$u = a_0 \frac{de_1}{dt} + k_0 \text{sgn}(s_1(e)) \quad \forall k_0 > 0 \quad (18)$$

From (9) and (18), the currents i_d and i_q are calculated as:

$$i_d = i_q = \frac{a_0 \frac{de_1}{dt} + k_0 \text{sgn}(s_1(e))}{K_f} \quad (19)$$

$$\forall a_0, k_0 > 0 \quad F - F_l = Ma$$

Thus, (19) is the SMC used for the position controller. Next, the speed controller is calculated correspondingly, but it has a difference from the reference signal.

C. Designing the Speed Controller

It is similar to the position controller, with settings [17]:

$$K_{T\omega} = \frac{K_T}{J} \text{ and } u_\omega = K_{T\omega} A_m \quad (20)$$

The controlled object is still a double integral $1/s^2$, but the feedback signal is state variable, thus, the sliding surface is chosen as:

$$s_\omega(e) = b_0 e_{1\omega} + e_{2\omega} = b_0 e_{1\omega} + \frac{de_{1\omega}}{dt} \quad (21)$$

where $e_{2\omega}$ is the speed error and b_0 is a positive design parameter.

Similar to the position controller, we have:

$$s_\omega \frac{ds_\omega}{dt} < 0 \Leftrightarrow \frac{ds_\omega}{dt} \text{sgn}(s_\omega(e)) < 0 \quad (22)$$

$$\Leftrightarrow u_\omega = \begin{cases} > b_0 \frac{de_{1\omega}}{dt} & if \quad s_\omega(e) > 0 \\ < b_0 \frac{de_{1\omega}}{dt} & if \quad s_\omega(e) < 0 \end{cases} \quad (23)$$

Choosing the control input u_ω as:

$$u = b_0 \frac{de_{1\omega}}{dt} + C.\text{sgn}(s_\omega(e)), \forall C > 0 \quad (24)$$

From (20) and (23), the current A_m is calculated as:

$$A_m = \frac{b_0 \frac{de_{1\omega}}{dt} + C.\text{sgn}(s_\omega(e))}{K_{T\omega}} \quad \forall b_0, C > 0 \quad (25)$$

Thus, (25) is the SMC which is used for the speed controller. The control system was designed from (19) and (24). However, to reduce the chattering due to the sgn(s) function, the sign function is replaced by the sat(s) function, which is defined as follows:

$$\text{sat}(s) = \begin{cases} \text{sgn}(s) & if \quad |s| > \varepsilon \\ \frac{s}{\varepsilon} & if \quad |s| \le \varepsilon \end{cases} \quad (26)$$

where ε is the boundary layer thickness. However, although the sliding mode can be guaranteed outside the ε, it cannot be guaranteed inside it. This replacement can cause trajectory errors.

To reduce both chattered phenomenon and trajectory error, a saturation-integral relay function (SatPi) is proposed which is defined as:

$$\text{SatPi}(s) = \begin{cases} \text{sgn}(s) & if \quad |s| > \varepsilon \\ \frac{s}{\varepsilon} + k_i \int_{t_0}^{t} s(t).dt & if \quad |s| \le \varepsilon \end{cases} \quad (27)$$

where k_i is positive integral coefficient, t_0 is the time when the system state starts to reach ε.

IV. EXPERIMENTS AND RESULTS

A. Setup

The entire experimental table is shown in Figure 4. Control Desk software was used to simulate models, build user interfaces, display process variables on screen, performing controller tuning, and monitoring objects. Table I presents the motors and the SMC controller parameters.

TABLE I.   SIMULATION PARAMETERS

Motor parameters	Symbol	Value
Motor weight	m	0.4 Kg
Rotor radius	R	0.022 m
Stator radius	r	0.027 m
Flux maximum of the rotor	B	0.59 T
Length of the parallel part	l_p	0.008 m
Length of the serial part	l_t	0.006 m
The total number of turns	n	55
Controller parameters	**Symbol**	**Value**
Current-torque coefficient	k_m	-9.7×10^{-4}
Current-torque coefficient	k_{nm}	52.5
Current-force coefficient	k_b	-0.0277
Current-force coefficient	k_{nb}	45.49
Position controller parameter	a_0	150
Position controller parameter	k_0	100
Speed controller parameter	b_0	92
Speed controller parameter	C	56
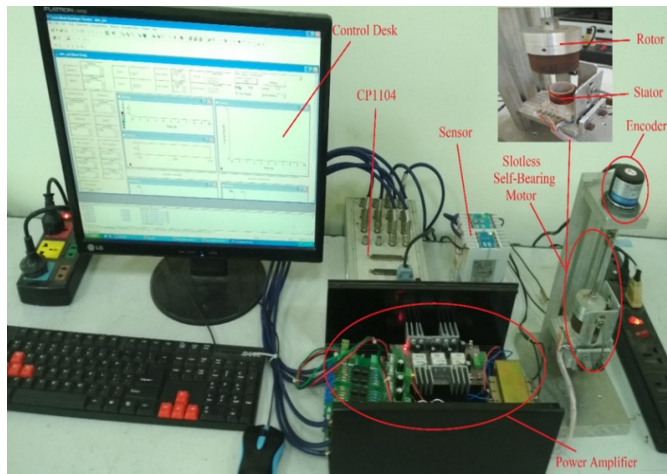
Fig. 4.   Images of the experimental version.

B. Results

The first tested controller was the position controller. The initial position of the rotor is $x = 0.5$mm, $y = 0.5$mm. At 0.8s the position controller was activated. The results are shown in Figure 5. At this point, the rotor position was brought back to the equilibrium position after only 0.12s, the currents i_d and i_q changed respectively and were limited from -1A to 1A.

After the position controller worked, the motor was brought to the balance position. Next, the rotor shaft was aligned with the origin, increasing the motor speed from 0 to 4500rpm. The results of the speed test response and change of rotor position are shown in Figure 6. The position response in the x and y axes has a slight fluctuation, but with minimal value. The most significant position deviation is only 0.1mm, thereby showing that the position controller works well even when the engine is running—motion at high speed.
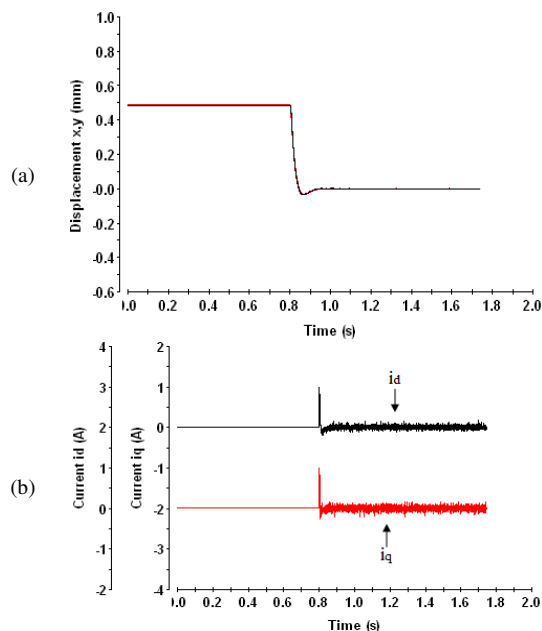
Fig. 5.   Experimental results of the position controller. (a) x, y axis position response (mm), (b) i_d, i_q current responses.
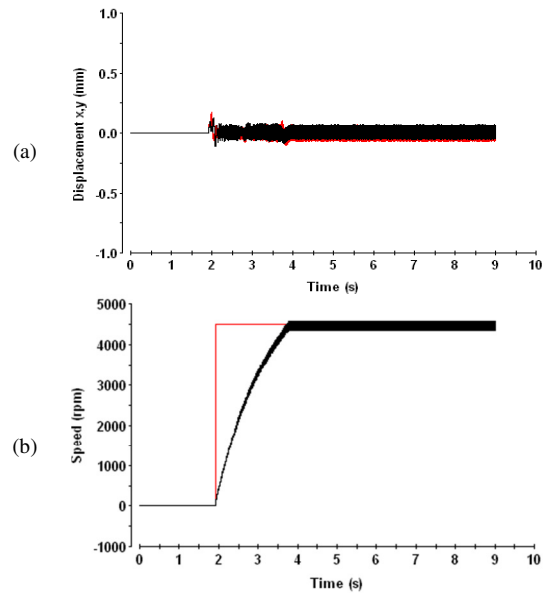
Fig. 6.   Position response when speed changes. (a) x, y axis position response (mm), (b) speed change from 0 to 4500rpm. The line red is the reference response, and the black line is the real response.
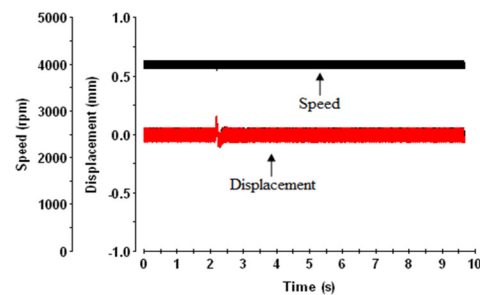
Fig. 7.   Response to position and speed in the presence of applied resistance.

To demonstrate that the position controller and speed controller work independently when the motor is operating at 4000rpm, a sufficient force is applied in both x and y axes of the engine. The actual speed response is close to the set speed response, without overturning, and the time it takes to set the speed is short (t=2s). At this point, the position error occurs, and immediately after that, the position controller suppresses the error and returns to 0rpm. The motor speed does not change, showing that speed and position controllers operate independently. Figure 8 shows the results of testing the rotor's trajectory at rotational speeds of 2000rpm and 4000rpm. Again, the maximum orbital deviation is approximately 0.12mm, and the engine operates stably. Figure 9 depicts the position deviation trajectory of the rotor along with the axis Ox (e_{1x}) and its derivative. Figure 9(a) shows the position error trajectory when the position controller starts to operate. At this time, the position error moves from 0.5mm to 0mm. Figure 9(b) shows that when the position controller is active, and the motor is stationary, the position error is approximately 0mm. Figure 9(c) shows the position deviation trajectory at 4000rpm. The maximum deviation amplitude is approximately 0.125mm. This value is relatively small, so we can say that the position controller is working correctly.
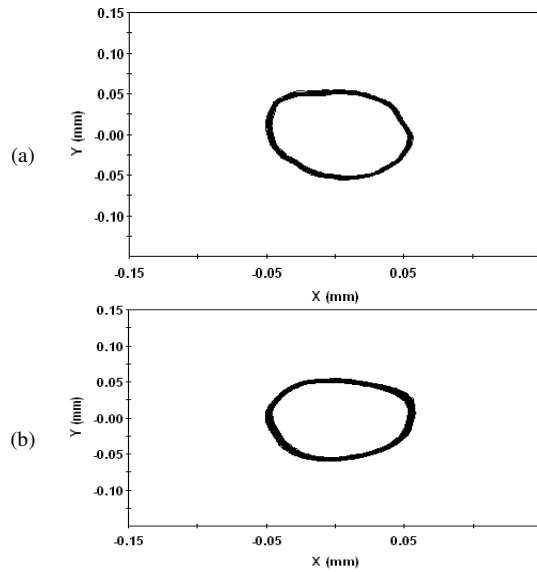
Fig. 8.   Response to position and speed in the presence of applied resistance: (a) 2000rpm, (b) 4000rpm.
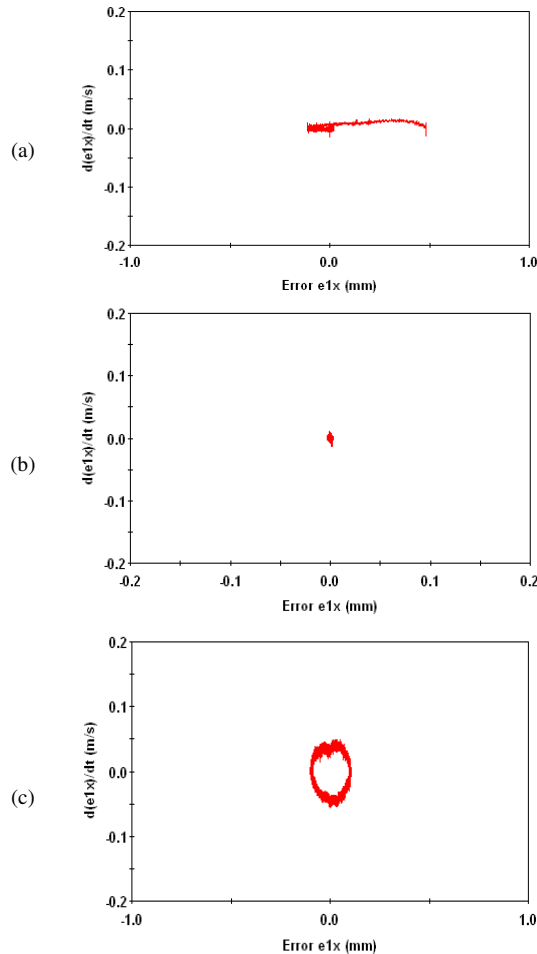
Fig. 9.   The trajectory of the rotor position deviation along the *x* axis: (a) initial starting position of controller response, (b) position response when the motor is stationary, (c) position response at 4000rpm.
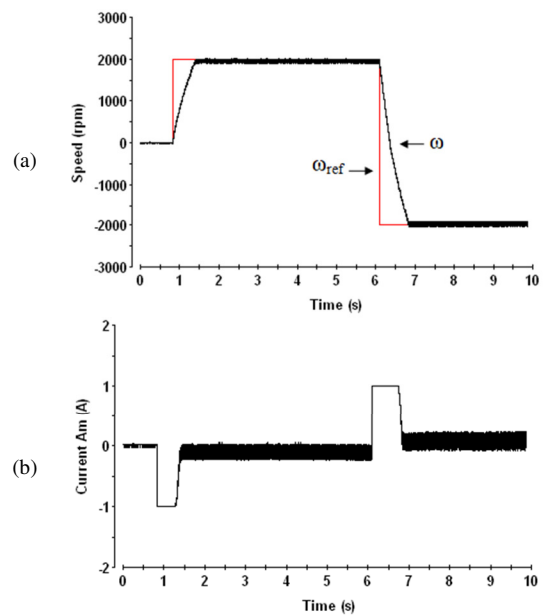
Fig. 10.   Experimental results of the speed controller: (a) Speed response, (b) current response.

Finally, the response of the speed controller, with increasing and decreasing speed of the motor, is tested. At 1s, the motor speed increased from 0rpm to 2000rpm, and at 6s, it reversed to -2000rpm. The corresponding A_m current and the speed responses were checked (A_m current is limited from -1A to 1A). The motor speed increases from 0 to 2000rpm after 0.5s and reverses after about 1s. The experimental results in Figure 10 show that the system works stably, and that the position and speed controllers work well. However, there are still errors and incompleteness as in the simulation, but the deviation is not too much. They are enough for the controller to be used to control the motor and they verify that the motor model is almost as accurate as the experimental.

V.   CONCLUSION

This article presents a detailed speed and position control design using SMC for SSBMs. The experimental results reliably verify the effectiveness of the proposed control method. In addition, it is shown that this motor is able to run stably at a considerable high-speed range with a small position error. Therefore, this research is a reasonable basis for controlling SSBMs with neural networks and fuzzy or artificial intelligence combined with state observers and tests in the future.

REFERENCES

[1]   Y. Okada, K. Dejima, and T. Ohishi, "Analysis and comparison of PM synchronous motor and induction motor type magnetic bearings," *IEEE Transactions on Industry Applications*, vol. 31, no. 5, pp. 1047–1053, Sep. 1995, https://doi.org/10.1109/28.464518.

[2]   Z. Ren and L. S. Stephens, "Closed-loop performance of a six degree-of-freedom precision magnetic actuator," *IEEE/ASME Transactions on Mechatronics*, vol. 10, no. 6, pp. 666–674, Sep. 2005, https://doi.org/10.1109/TMECH.2005.859823.

[3]   T. Schneider and A. Binder, "Design and Evaluation of a 60 000 rpm Permanent Magnet Bearingless High Speed Motor," in *7th International Conference on Power Electronics and Drive Systems*, Bangkok, Thailand, Nov. 2007, pp. 1–8, https://doi.org/10.1109/PEDS.2007.4487669.

[4]   Q. D. Nguyen and S. Ueno, "Analysis and Control of Nonsalient Permanent Magnet Axial Gap Self-Bearing Motor," *IEEE Transactions on Industrial Electronics*, vol. 58, no. 7, pp. 2644–2652, Jul. 2011, https://doi.org/10.1109/TIE.2010.2076309.

[5]   Q. D. Nguyen and S. Ueno, "Modeling and Control of Salient-Pole Permanent Magnet Axial-Gap Self-Bearing Motor," *IEEE/ASME Transactions on Mechatronics*, vol. 16, no. 3, pp. 518–526, Jun. 2011, https://doi.org/10.1109/TMECH.2010.2045392.

[6]   S. Ueno, R. Iseki, and C. Jiang, "Stability of a tilt-controlling axial gap self-bearing motor with single-stator," *Mechanical Engineering Journal*, vol. 4, no. 4, 2017, Art. no. 16-00337, https://doi.org/10.1299/mej.16-00337.

[7]   R. Qu, M. Aydin, and T. A. Lipo, "Performance comparison of dual-rotor radial-flux and axial-flux permanent-magnet BLDC machines," in *IEEE International Electric Machines and Drives Conference*, Madison, WI, USA, Jun. 2003, vol. 3, pp. 1948–1954, https://doi.org/10.1109/IEMDC.2003.1210718.

[8]   A. O. Salazar, "A Review of Developments in Bearingless Motors," in *Seventh International Symposium on Magnetic Bearings*, Zurich, Switzerland, Aug. 2000, pp. 335–340.

[9]   S. Yajima, M. Takemoto, Y. Tanaka, A. Chiba, and T. Fukao, "Total Efficiency of a Deeply Buried Permanent Magnet Type Bearingless Motor Equipped with 2-pole Motor Windings and 4-pole Suspension Windings," in *IEEE Power Engineering Society General Meeting*, Tampa, FL, USA, Jun. 2007, pp. 1–7, https://doi.org/10.1109/PES.2007.386109.

[10] H. Grabner, W. Amrhein, S. Silber, and W. Gruber, "Nonlinear Feedback Control of a Bearingless Brushless DC Motor," *IEEE/ASME Transactions on Mechatronics*, vol. 15, no. 1, pp. 40–47, Oct. 2010, https://doi.org/10.1109/TMECH.2009.2014058.

[11] D. Steinert, T. Nussbaumer, and J. W. Kolar, "Slotless Bearingless Disk Drive for High-Speed and High-Purity Applications," *IEEE Transactions on Industrial Electronics*, vol. 61, no. 11, pp. 5974–5986, Aug. 2014, https://doi.org/10.1109/TIE.2014.2311379.

[12] D. Steinert, T. Nussbaumer, and J. W. Kolar, "Evaluation of One- and Two-Pole-Pair Slotless Bearingless Motors With Toroidal Windings," *IEEE Transactions on Industry Applications*, vol. 52, no. 1, pp. 172–180, Jan. 2016, https://doi.org/10.1109/TIA.2015.2466683.

[13] Y. L. Karnavas and I. D. Chasiotis, "PMDC coreless micro-motor parameters estimation through Grey Wolf Optimizer," in *XXII International Conference on Electrical Machines*, Lausanne, Switzerland, Sep. 2016, pp. 865–870, https://doi.org/10.1109/ICELMACH.2016.7732627.

[14] I. Stamenkovic, N. Milivojevic, N. Schofield, M. Krishnamurthy, and A. Emadi, "Design, Analysis, and Optimization of Ironless Stator Permanent Magnet Machines," *IEEE Transactions on Power Electronics*, vol. 28, no. 5, pp. 2527–2538, Feb. 2013, https://doi.org/10.1109/TPEL.2012.2216901.

[15] S. Ueno, S. Uematsu, and T. Kato, "Development of a Lorentz-Force-Type Slotless Self-Bearing Motor," *Journal of System Design and Dynamics*, vol. 3, no. 4, pp. 462–470, 2009, https://doi.org/10.1299/jsdd.3.462.

[16] S. Ueno and T. Kato, "A novel design of a Lorentz-force-type small self-bearing motor," in *International Conference on Power Electronics and Drive Systems*, Taipei, Taiwan, Nov. 2009, pp. 926–931, https://doi.org/10.1109/PEDS.2009.5385835.

[17] H. P. Nguyen, X. B. Nguyen, T. T. Bui, S. Ueno, and Q. D. Nguyen, "Analysis and Control of Slotless Self-Bearing Motor," *Actuators*, vol. 8, no. 3, Sep. 2019, Art. no. 57, https://doi.org/10.3390/act8030057.

[18] S. Kobayashi, M. Ooshima, and M. N. Uddin, "A radial position control method of bearingless motor based on d-q axis current control," *IEEE Transactions on Industry Applications*, vol. 4, no. 49, pp. 1827–1835, 2013, https://doi.org/10.1109/TIA.2013.2257972.

[19] G. Boztas, M. Yildirim, and O. Aydogmus, "Design and Analysis of Multi-Phase BLDC Motors for Electric Vehicles," *Engineering, Technology & Applied Science Research*, vol. 8, no. 2, pp. 2646–2650, Apr. 2018, https://doi.org/10.48084/etasr.1781.

[20] D. M. Duc, T. X. Tuy, and P. D. Phuoc, "A Study on the Response of the Rehabilitation Lower Device using Sliding Mode Controller," *Engineering, Technology & Applied Science Research*, vol. 11, no. 4, pp. 7446–7451, Aug. 2021, https://doi.org/10.48084/etasr.4312.

[21] T. L. Nguyen, T. H. Vo, and N. D. Le, "Backstepping Control for Induction Motors with Input and Output Constrains," *Engineering, Technology & Applied Science Research*, vol. 10, no. 4, pp. 5998–6003, Aug. 2020, https://doi.org/10.48084/etasr.3680.

[22] M. Ooshima, S. Kobayashi, and M. N. Uddin, "Magnetic levitation tests of a bearingless motor based on d-q axis current control," in *IEEE Industry Applications Society Annual Meeting*, Las Vegas, NV, USA, Oct. 2012, pp. 1–7, https://doi.org/10.1109/IAS.2012.6374033.

[23] J.-J. Slotine and W. Li, *Applied Nonlinear Control*. London, UK: Pearson, 1991.

[24] N. F. Al-Muthairi and M. Zribi, "Sliding mode control of a magnetic levitation system," *Mathematical Problems in Engineering*, vol. 2004, no. 2, pp. 93–107, 2004, https://doi.org/10.1155/S1024123X04310033.

[25] V. Utkin, "Variable structure systems with sliding modes," *IEEE Transactions on Automatic Control*, vol. 22, no. 2, pp. 212–222, Apr. 1977, https://doi.org/10.1109/TAC.1977.1101446.

[26] C. J. Fallaha, M. Saad, H. Y. Kanaan, and K. Al-Haddad, "Sliding-Mode Robot Control With Exponential Reaching Law," *IEEE Transactions on Industrial Electronics*, vol. 58, no. 2, pp. 600–610, Oct. 2011, https://doi.org/10.1109/TIE.2010.2045995.

[27] H.-M. Chin and L. S. Stephens, "Closed Loop Performance of a Slotless Lorentz Self-Bearing Motor," in *International Joint Power Generation Conference*, Atlanta, GA, USA, Feb. 2009, pp. 583–591, https://doi.org/10.1115/GT2003-38750.

[28] B. Azhari, P. Irasari, and P. Widianto, "Design and simulation of 5kW BLDC motor with half-buried permanent magnets using an existing stator body," *International Journal of Power Electronics and Drive Systems*, vol. 12, no. 4, pp. 2030–2043, 2021, https://doi.org/10.11591/ijpeds.v12.i4.pp2030-2043.

[29] R. Gunawan, F. Yusivar, and B. Yan, "The self excited induction generator with observation magnetizing characteristic in the air gap," *International Journal of Power Electronics and Drive Systems*, vol. 5, no. 3, pp. 355–365, 2015, https://doi.org/10.11591/ijpeds.v5.i3.pp355-365.

[30] N. Baharudin and S. M. Ayob, "Brushless DC Motor Speed Control Using Single Input Fuzzy PI Controller," *International Journal of Power Electronics and Drive Systems*, vol. 9, no. 4, pp. 1952–1966, Dec. 2018, https://doi.org/10.11591/ijpeds.v9.i4.pp1952-1966.

[31] A. Hinda, M. Khiat, and Z. Boudjema, "Advanced control scheme of a unifiedpower flow controller using sliding mode control," *International Journal of Power Electronics and Drive System*, vol. 11, no. 2, pp. 625–633, 2020, https://doi.org/10.11591/ijpeds.v11.i2.pp625-633.

[32] J.-W. Cheon, S.-B. Choi, H.-J. Song, and J.-H. Ham, "Position Control of an AC Servo Motor Using Sliding Mode Controller with Disturbance Estimator," *International Journal of Precision Engineering and Manufacturing*, vol. 5, no. 4, pp. 14–20, Oct. 2004.

[33] S. Navaneethan and J. Jovitha, "Speed control of Permanent Magnet Synchronous Motor using Power Reaching Law based Sliding Mode Controller," *Weas Transaction on Systems and Control*, vol. 10, pp. 270–277, 2015.

[34] M. A. Khlifi, M. B. Slimene, A. Alradedi, and S. A. Ahmadi, "Investigation of a Leakage Reactance Brushless DC Motor for DC Air Conditioning Compressor," *Engineering, Technology & Applied Science Research*, vol. 12, no. 2, pp. 8316–8320, Apr. 2022, https://doi.org/10.48084/etasr.4762.